November 1, 2005

Assimilative modeling of the equatorial ionosphere for scintillation forecasting: Modeling with vertical drifts

J. M. Retterer
D. T. Decker
W. S. Borer
R. E. Daniell
Bela G. Fejer, *Utah State University*

Assimilative modeling of the equatorial ionosphere for scintillation forecasting: Modeling with vertical drifts

John M. Retterer, D. T. Decker, and W. S. Borer
Air Force Research Laboratory, Space Vehicles Directorate, Hanscom Air Force Base, Massachusetts, USA

R. E. Daniell, Jr.
Computational Physics, Inc., Springfield, Virginia, USA

B. G. Fejer
Center for Space Sciences, Utah State University, Logan, Utah, USA

Received 29 July 2002; revised 17 November 2004; accepted 1 September 2005; published 19 November 2005.

[1] Knowledge of the vertical plasma drift velocity observed by the Jicamarca incoherent radar in seven events is assimilated into a theoretical model for the ambient *F* region plasma density. Comparisons of the calculated plasma density model and the observed plasma density show that, apart from the signature effects of equatorial plasma bubbles, the ambient model captures much of the detail of the plasma density profiles. Rayleigh-Taylor growth rates calculated with the ambient model show a good correlation with the occurrence of spread *F*.

Citation: Retterer, J. M., D. T. Decker, W. S. Borer, R. E. Daniell Jr., and B. G. Fejer (2005), Assimilative modeling of the equatorial ionosphere for scintillation forecasting: Modeling with vertical drifts, *J. Geophys. Res.*, *110*, A11307, doi:10.1029/2002JA009613.

1. Introduction

[2] Among the many highly variable drivers that control the occurrence of equatorial spread *F* on a given evening, it is generally agreed that few are as crucial as the vertical velocity in the prereversal enhancement following sunset, which determines how high the *F* layer rises into a region where collision frequencies are low and the growth rate for the generalized Rayleigh-Taylor instability is large [see, e.g., *Kelley*, 1989]. Correlations have been demonstrated between the peak vertical velocity and the occurrence of spread *F* [*Fejer et al.*, 1999] and between the height of the *F* layer and the onset of spread *F* [*Farley et al.*, 1970; *Sales*, 1999].

[3] Progress in modeling these phenomena has lagged, however, because the most complete and useful models of the vertical velocity are empirical models [e.g., *Scherliess and Fejer*, 1999], which describe the climatological variation of the velocity but are not meant to describe much of its day-to-day variability. The overplots of the vertical velocity in events from a database of Jicamarca observations [*Scherliess and Fejer*, 1999] show how variable this velocity can be. The empirical models are generally parameterized in terms of the solar 10.7 cm radio flux (and for a storm-time model [*Fejer and Scherliess*, 1997], the *AE* geomagnetic activity index). The daily variability of these indices leads to some day-to-day variability of the velocity, but since the empirical models were created by averaging much data to find the mean trends in noisy data and create smooth curves, they cannot capture most of the variability.

0148-0227/05/2002JA009613

[4] The vertical drift of the plasma as observed over a 24 hour period by the Jicamarca incoherent-scatter radar has been used to drive a theoretical model for the plasma density [*Preble et al.*, 1994], showing for one event that knowing the vertical drift greatly improves the accuracy of the modeling of the density profile. That study, however, did not address the consequences for the prediction of scintillations. We take up the study at this point, assimilating Jicamarca data from seven cases into an enhanced version of the AFRL theoretical model of the equatorial plasma density [*Anderson*, 1973] to study the accuracy of the resulting predictions for the ambient plasma density and calculate the Rayleigh-Taylor growth rates and look for systematic correlations between the daily occurrence and predictions of spread *F*.

2. Data

[5] The Jicamarca incoherent scatter radar (11.95°S, 76.87°W geographic, magnetic dip 2°N) has been used extensively for ionospheric studies since 1968 [*Farley*, 1991]. Details about the radar, its operations, and methods of observations and data analysis may be found in several publications (e.g., *McClure et al.* [1970] and *Farley* [1991] for operations; *Woodman and Hagfors* [1969] for details on the vertical drift technique). An extensive review of the vertical drifts observed by the Jicamarca radar may be found in work by *Fejer* [1991] and *Fejer et al.* [1991]. For this study, data from 7 days are used. They include equinoctal days in 1970 (30 September to 1 October, 1–2 October, 2–3 October) and 1971 (21–22 September, 22–23 September, 23–24 September) as well as one nonequinoctal day (23–24 July 1971). Solar conditions

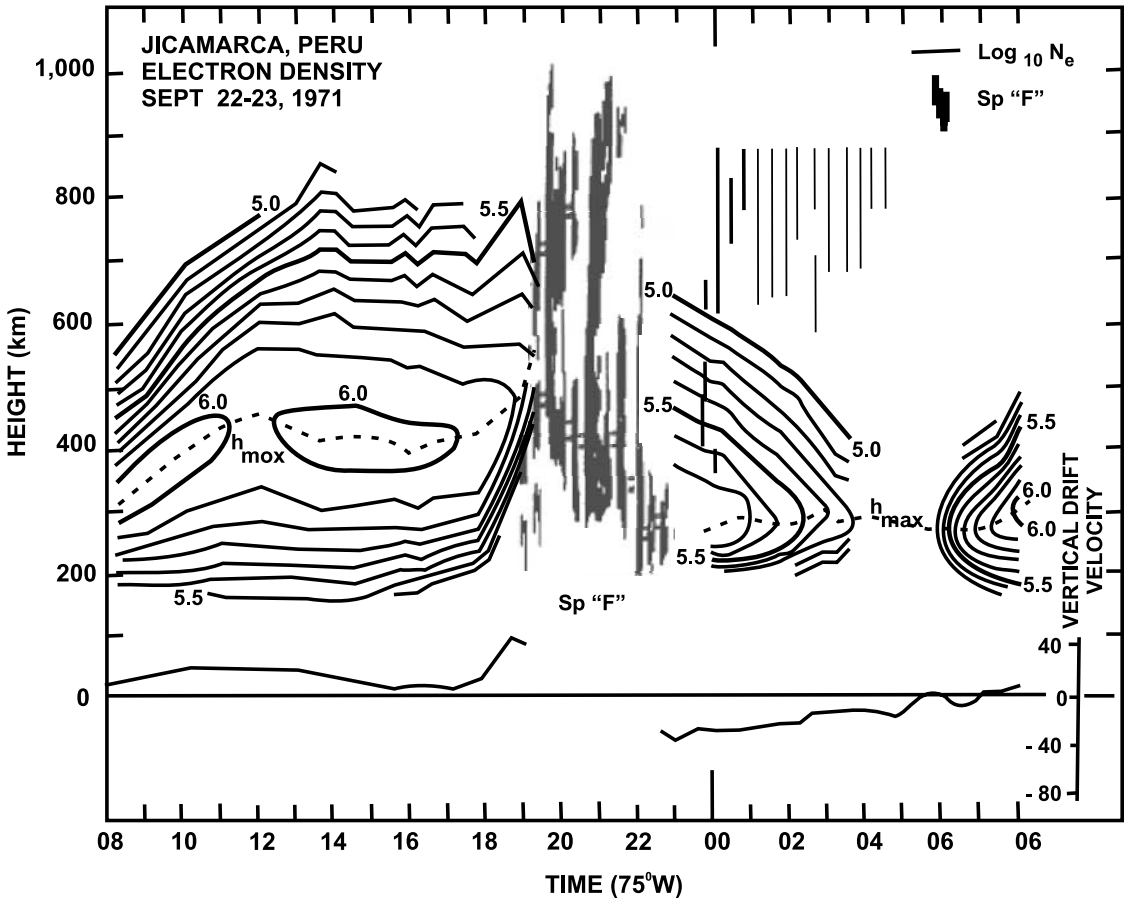

Figure 1. (top) Plasma density contour plot and (bottom) vertical drift velocity (in m/s) measured by the Jicamarca incoherent-scatter radar on 22 September 1971.

were moderate with the daily 10.7 cm radio flux ranging between 106 and 134 units and the magnetic activity was quiet with *Ap* ranging between 2 and 14.

[6] Figure 1 shows a contour plot of the plasma density measured on 22–23 September 1971 over Jicamarca, with the contour values in a logarithmic scale. The height resolution of the electron density and plasma drift measurements was about 20–30 km and the integration time was about 10–15 min. The estimated error in density for these contours is less than 5% for densities greater than 10^4 electrons cm^{-3} [*McClure et al.*, 1970]. The dashed line represents the peak layer height (h_mF_2) and traces the diurnal variations of the peak electron concentration (N_mF_2). The irregular patches following sunset denotes the occurrence of equatorial spread *F*, which masks the incoherent scatter signal [*Farley et al.*, 1970; *Woodman and LaHoz*, 1976].

[7] The observed *F* region vertical plasma drift velocity (in meters per second) is presented at the bottom of Figure 1. The positive values indicate upward drifts (driven by an eastward electric field). The vertical drifts for this day fall within the expected range of the drifts under solar moderate equinoctal conditions, as categorized by *Fejer et al.* [1991]. However, the peak prereversal velocity is larger than the value of the empirical drift model appropriate for the day. While this day had the largest peak prereversal drift of the seven, all 7 days had peak drifts larger than the climatological values and had some spread *F* activity.

3. Low-Latitude Ambient Plasma Density Model

[8] The AFRL low-latitude ionospheric model solves the O^+ continuity equation as a function of position along a field line and time for a series of flux tubes over a range of field-line apex altitudes so as to be able to specify the O^+ density as a function of altitude and latitude at a specific longitude and time. It is based on the LOWLAT model of Anderson, used by *Preble et al.* [1994], and uses the techniques referred to there to solve the continuity equation. This variety of plasma model does not consider the self-consistent fields of plasma perturbations, so it describes the ambient plasma, unperturbed by the generation of plasma structure by plasma instabilities. This plasma model thus provides a zeroth-order state which can be used for an analysis of plasma instability or used as the initial state of a nonlinear study of the development of the plasma structures that lead to equatorial bubbles. Instead of the tilted dipole coordinate system commonly used in versions of LOWLAT, the new AFRL model uses field lines traced from the IGRF model of the geomagnetic field.

[9] In order to solve the continuity equation, the following input parameters must be specified as functions of

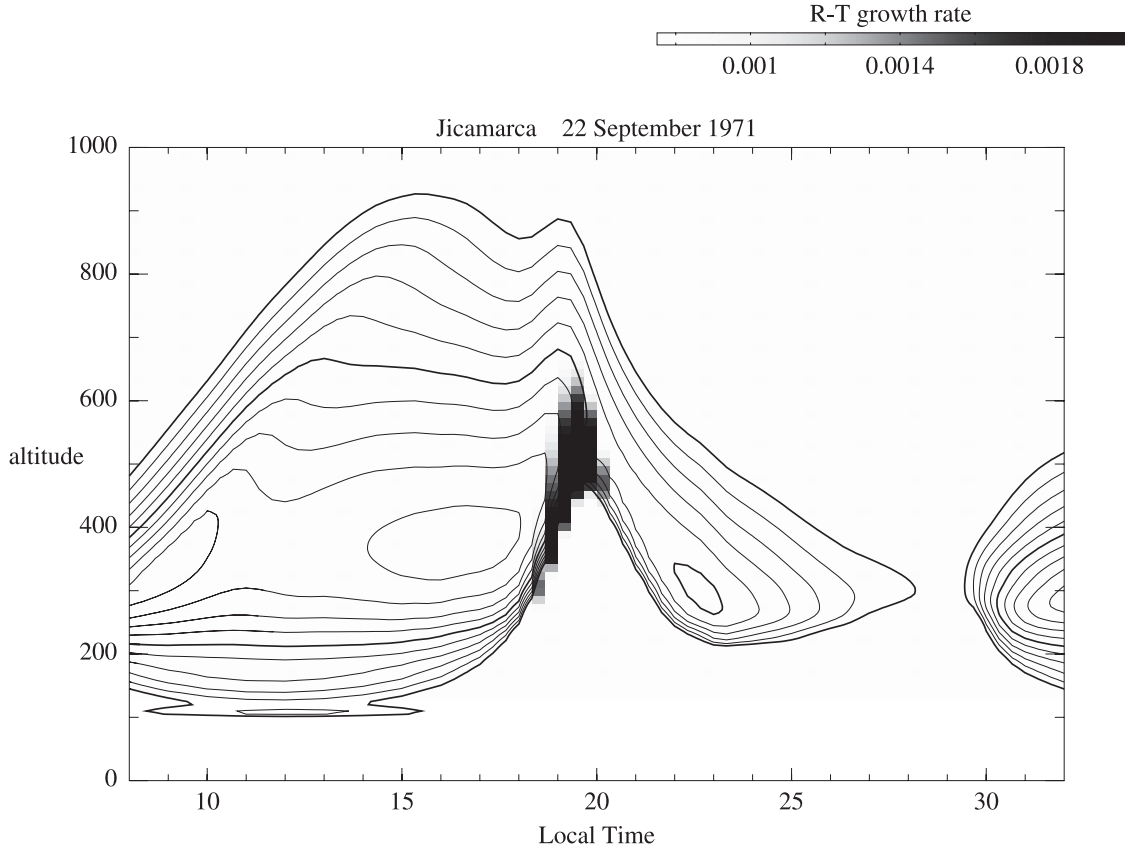

Figure 2. Plasma density contour plot, with a color-scale plot of Rayleigh-Taylor growth rate superimposed, for 22 September 1971. The contours are drawn for log (base 10) densities equal to 5 (the outermost contour), 5.1, 5.2,.... See color version of this figure in the HTML.

altitude, location, time, solar activity, and geomagnetic activity:

[10] 1. The neutral atmospheric densities of N_2, O_2, and O, and the neutral temperature, are obtained from the MSIS model of *Hedin* [1987].

[11] 2. The horizontal neutral wind components are obtained from the empirical wind model HWM-90 of *Hedin et al.* [1991]. No vertical wind is assumed.

[12] 3. The ion and electron temperatures are based on the empirical model of *Brace and Theis* [1981].

[13] 4. Production and loss rates of O^+ are calculated from the local model of *Jasperse* [1974]; production rates used the solar EUV fluxes derived from the algorithm of *Hinteregger* [1981].

[14] 5. Zonal ion drifts are given by the empirical model of *Fejer* [1991], based on Jicamarca observations. In this paper we have knowledge of the vertical ion drifts; in other circumstances, when vertical $\mathbf{E} \times \mathbf{B}$ drift velocity information is not available, we use the empirical drift models [*Scherliess and Fejer*, 1999] based on observations from Jicamarca and the AE-E satellite.

[15] Figure 2 shows the results of the O^+ density calculated through the course of the Jicamarca observations of 22–23 September 1971, using the measured vertical drift as a driver for the calculation. We see that the calculation captures most of the details of the observed density (see Figure 1): the buildup of the plasma density in the morning, and the sudden lifting of the *F* layer following 1800 LT, and then the decay of the density after midnight. Without any adjustments of the parameters of the model, particularly the temperatures, neutral winds, and height variation of the electric field, this model does not describe all the details of the plasma density structure seen in Figure 1, but it certainly describes the overall structure well. (Note that some of the lower-density or finer-scale features seen in the model calculation, such as the structure below 200 km in the daytime and the topside densities may be present in the observations but could not be resolved by the radar.) Our predictions of scintillation activity are most sensitive to the structure near the lower boundary of the plasma, where the model describes the observations quite well.

[16] The case presented in Figures 1 and 2 represents the most active in terms of scintillation strength of the seven cases available in this study. In contrast, Figures 3 and 4 present the data and density calculation for 23–24 July 1971, when the scintillation was the weakest and lasted the shortest length of time. Figure 3 presents the Jicamarca data, for both the density (top) and plasma drift (bottom) as a function of local time. The cross-hatched area indicates the time of bottomside spread *F* scintillation. We see that the peak vertical drift in the prereversal enhancement on this day near June solstice is smaller than that of the equinoctal day shown in Figure 1, which is usually the case. Figure 4 shows the resulting plasma density calculation when the observed plasma drift is assimilated into the AFRL model.

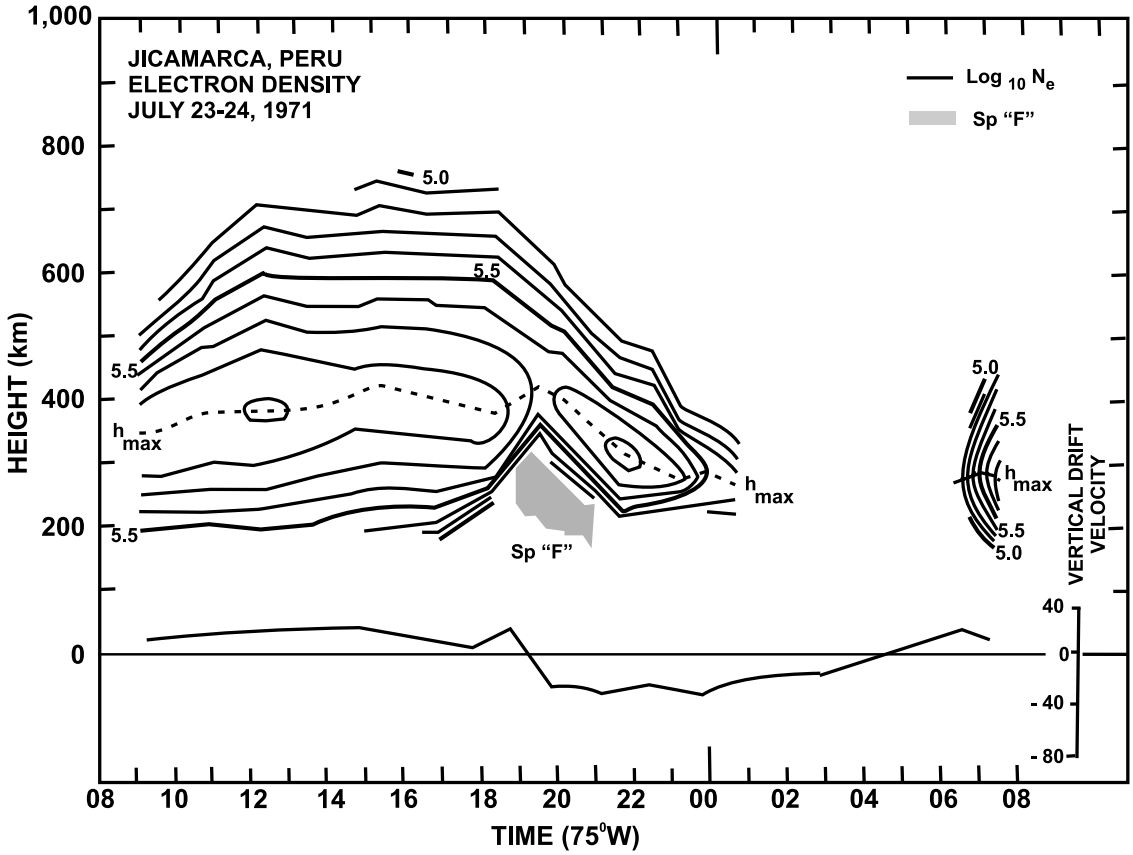

Figure 3. (top) Plasma density contour plot and (bottom) vertical drift velocity (in m/s) measured by the Jicamarca incoherent-scatter radar on 23 July 1971.

We see that the height of the bottomside edge of the *F* layer is again well described by the model.

4. Rayleigh-Taylor Growth Rates

[17] The linear theory of the Rayleigh-Taylor instability and the calculation of its growth rate has been discussed extensively by *Sultan* [1996], based on the magnetic flux-tube formalism of *Haerendel et al.* [1992]. The linear growth rate gives the exponential rate at which a perturbation in the plasma will grow as long as the perturbation remains small. Important points incorporated in the Sultan formulation include integration of properties of the plasma along the flux tube, and inclusion of the effects of ionospheric electric fields, neutral winds, and a finite-density *E* region.

[18] A calculation of the linear growth rate of a perturbation is based on an assumption of a form for the perturbation. The Haerendel/Sultan formulation assumes that the perturbation is uniform in amplitude all along the flux tube. An alternative formulation permits the perturbation mode to possess some structure along the field line [*Basu and Coppi*, 1983], e.g., to be peaked at the geomagnetic equator. A flux-tube integrated formulation of the calculation of the linear growth rate, permitting such variation (but in this application evaluated with a uniform profile), was given by *Rappaport* [1996]. The linear growth rates we present were calculated using the Rappaport formulation, extended as *Sultan* [1996] did to include the effects of ionospheric electric fields and neutral winds. In practice, with the Rappaport formula evaluated with a uniform mode amplitude, the quantitative differences between the Sultan and Rappaport results were small. See Appendix A for the detailed formula of the growth rate calculated here.

[19] The significance of the terms in the growth-rate formula have been described perhaps most completely by *Sultan* [1996]. As formula (A5) suggests, the growth rate is proportional to an integral of the density gradient perpendicular to the geomagnetic field in a direction which is outward from the Earth at the geomagnetic equator (the α direction), so the growth rate is enhanced for the field line which passes through the sharp density gradient at the bottomside of the *F* region. The growth rate is also inversely proportional to an integral of the Pedersen conductivity, so is enhanced when the flux tube is lifted in altitude to where the ion-neutral collision frequency is small. The growth rate is, in addition, proportional to an acceleration in the α direction and so is enhanced where the zonal electric field or vertical neutral wind is bigger.

[20] The linear growth rate of the generalized Rayleigh-Taylor instability was calculated using the model plasma density profiles and other model information. Grayscale plots of the value of the linear growth rate as a function of local time and apex altitude in the 22–23 September 1971 and 23–24 July 1971 events are superimposed on the density picture in Figures 2 and 4, respectively. The 22 September 1971 event produced the strongest growth

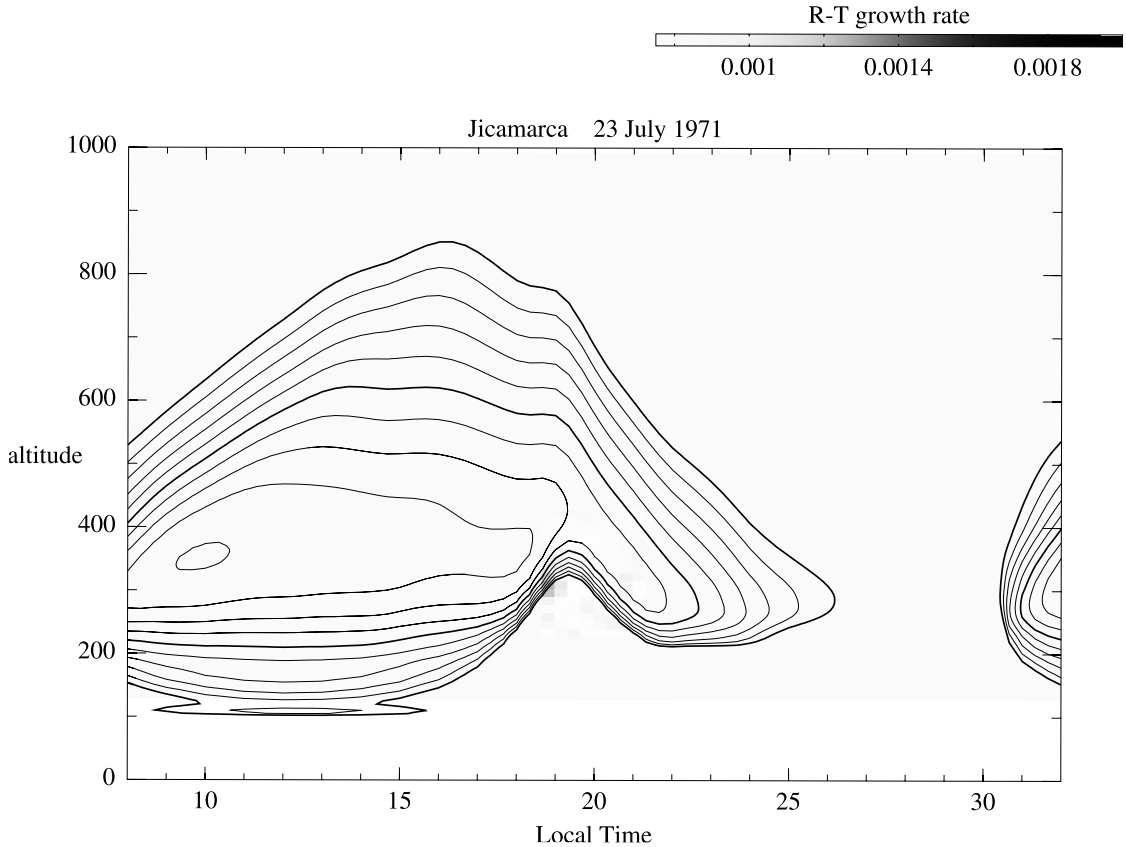

Figure 4. Plasma density contour plot, with a color-scale plot of Rayleigh-Taylor growth rate superimposed, for 23 July 1971. The contours are drawn for log (base 10) densities equal to 5 (the outermost contour), 5.1, 5.2,. . .. See color version of this figure in the HTML.

rates of the seven cases, with a peak growth rate of over 0.003 s^{-1} or an exponentiation time less than 5 min. Figure 4, on the other hand, shows us that the peak growth rate in the 23 July 1971 event was much smaller, just barely visible around 1900 LT.

[21] A summary of the peak growth rates calculated for all seven events is shown in Figure 5. The black points are the results of calculations using the observed vertical drifts, while the gray points are the results using a climatological [*Scherliess and Fejer*, 1999] model. The upper left panel shows the peak growth rate correlated with the maximum vertical drift in the prereversal enhancement, and we see a more-or-less one-to-one correspondence between the maximum vertical velocity and the peak growth rate. Note also that the results with the climatological drifts fall on the same curve, but since the actual drifts in all seven cases were larger than the climatological predictions for the drifts, the growth rates were smaller than the growth rates calculated with the actual drifts. Some of the scatter of the growth-rate values may be attributed to the timing of the peak velocity; the same peak velocity at somewhat different local times can give rise to different uplifts and growth rates.

[22] The upper right panel shows the correlation between peak growth rate and the altitude of the maximum vertical density gradient, which corresponds to the sharp lower edge of the lifted *F* layer (h′F). It appears that there is slightly more scatter among the data points; the correlation is not quite as good as the correlation with the peak vertical drift. If this difference is borne out in more complete surveys, it may be due to the fact that in addition to controlling the height of the *F* layer, the zonal electric field contributes directly to the growth rate, improving the correlation seen in the left panel. Another point is that the growth rate depends on the gradient of the flux-tube-integrated content, not the gradient of the density, and there may be slight differences between the heights of the peaks of the two functions.

[23] The lower left panel shows the correlation between peak growth rate and the solar 10.7 cm radio flux parameter, F10.7. Over the narrow range of F10.7 in the events of this study, there is little apparent correlation between F10.7 and the peak growth rate.

[24] The lower right panel shows the correlation between F10.7 and maximum vertical drift, plotting the same variables analyzed by *Fejer et al.* [1999]. Instead of indicating for each event whether spread *F* was observed (in these events, spread *F* in some degree was observed in all of them), we make the size of the point vary proportionally with the magnitude of the peak growth rate calculated for the event. We find the events with the strongest growth rates at the top of the figure, almost independent of the F10.7 parameter, but showing again the good correlation between peak velocity and growth rate. The study of *Fejer et al.* [1999] included events from a wider range of F10.7, and there it appears that the threshold of vertical velocity for the occurrence of spread *F* increased with F10.7. This may be

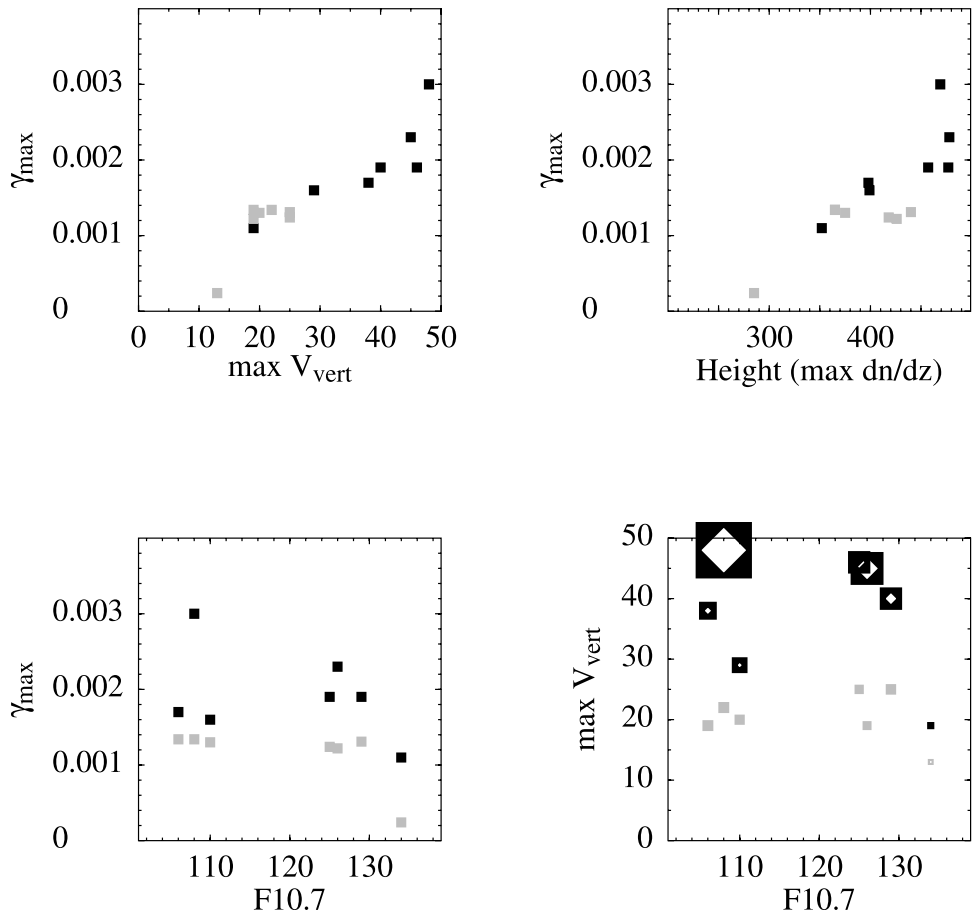

Figure 5. Peak values of the Rayleigh-Taylor growth rate for each of the seven events, correlated against (a) the peak vertical drift velocity in the prereversal enhancement, (b) the altitude of the maximum density gradient with respect to height, (c) F10.7, and (d) the correlation between the peak vertical drift and F10.7, with the size of the points scaled with the growth rate. The black points are derived from the calculations performed with the measured vertical drift and the gray points are derived from calculations performed with the climatological drifts.

explained by the effect of F10.7 on other aspects of the ionosphere. Increased F10.7 gives a higher neutral temperature, leading to a higher neutral density, higher collision frequency, and reduced growth rate for a given vertical drift.

5. Bubble Formation

[25] The trend of bubble or spread *F* formation among the seven cases is consistent with the growth rates calculated. The case in which coherent echoes from plasma turbulence in bubbles was observed was the case for which the calculated growth rate was the highest, while the case for which the growth rate was weakest (and positive for the shortest time) was a case in which only bottomside spread *F* was observed.

[26] To follow the development of the plasma perturbations beyond the stage when their amplitudes are small, however, a nonlinear model of the plasma is required [*Ossakow*, 1981]. A new model [*Retterer*, 1999], based on the principles of the NRL model [*Zalesak et al.*, 1982] but elaborated to include more of the details of the background ionosphere, has been developed to study the development of equatorial plasma depletions after sunset. The model follows the temporal evolution of the plasma density in the *F* region, with self-consistent electric fields, using the nonlinear continuity, momentum, and current-conservation equations. This model will be used in subsequent reports to describe the development of bubbles in the unstable ionospheric plasma found in the present study.

6. Conclusions

[27] The main conclusion we draw from this study is that knowledge of the vertical drift velocity in the prereversal enhancement is essential for predicting the occurrence of spread *F* in the evening sector, reinforcing the conclusion drawn from empirical studies [*Fejer et al.*, 1999]. We found that when the theoretical model assimilated knowledge of this velocity into the calculation of the plasma density, the model did an excellent job of predicting the structure of the ambient density. Rayleigh-Taylor growth rates calculated with this density structure were well ordered with respect to the occurrence of spread *F* (among the seven cases we studied): the event with the smallest predicted growth rate had the weakest spread *F*, and the event with the highest growth rate had the strongest.

[28] The correlation between growth rate and peak drift velocity was much stronger than the correlation between growth rate and proxies such as the F10.7 index. These cases were selected over only a small range of F10.7, however, and it will be useful to extend the study to include more events over a wider range of conditions.

[29] We also look forward to assimilating other sources of data for the plasma, such as the in situ density and velocity measurements planned for the C/NOFS mission [*de la Beaujardiere et al.*, 2004], to better forecast the occurrence of spread *F*.

Appendix A: Growth-Rate Formula

[30] We consider first the dipole approximation to the geomagnetic field, and work in the dipole coordinate system, with coordinates labeled (α, β, δ), defined in terms of spherical coordinates as

$$\alpha = \frac{r/\mathrm{R_E}}{\sin^2\theta}, \qquad \beta = \phi, \qquad \delta = \frac{\cos\theta}{(r/\mathrm{R_E})^2}, \tag{A1}$$

where (r, θ, ϕ) are the radius, colatitude, and longitude in the spherical system with pole aligned with the Earth's magnetic pole, and $\mathrm{R_E}$ is the Earth's radius. Thus α and β label the field line, and δ identifies the position along the field line. At the magnetic equator, α is radially outward ("up"). These coordinates form an orthogonal curvilinear coordinate system [*Morse and Feshbach*, 1953], with scale factors

$$h_\alpha = \frac{\mathrm{R_E}\sin^3\theta}{\Delta}, \qquad h_\beta = r\sin\theta, \qquad h_\delta = \frac{r^3}{\mathrm{R_E^2}\Delta}, \tag{A2}$$

where $\Delta \equiv (1 + 3\cos^2\theta)^{\frac{1}{2}}$. The flux-tube integral of a quantity $q(\alpha, \beta, \delta)$ is defined to be

$$I(q) = \frac{1}{\mathrm{R_E^2}} \int q(\alpha,\beta,\delta) h_\alpha h_\beta h_\delta d\delta. \tag{A3}$$

[31] Choosing plasma perturbations to be of the form

$$\psi(\delta)\exp(iK_L\alpha + im\beta)\exp(\gamma t) \tag{A4}$$

with the amplitude ψ assumed to be constant except at the ends of the field line, where it goes to zero rapidly, *Rappaport*'s [1996] linear-mode analysis gives the growth rate

$$\gamma = \frac{I(w_2)}{I(w_1)}, \tag{A5}$$

where the integrands for the flux-tube integrals are

$$w_1 = \left(\frac{K_L^2}{h_\alpha^2} + \frac{m^2}{h_\beta^2}\right)\sigma_P, \tag{A6}$$

and

$$w_2 = \frac{-M_i}{B^2} A_\alpha \frac{1}{h_\alpha}\frac{\partial n}{\partial \alpha}\frac{m^2}{h_\beta^2}. \tag{A7}$$

Here σ_P is the Pedersen conductivity, M_i is the ion mass, B is the magnitude of the geomagnetic field, n is the ion density, and A_α is an acceleration in the α direction, which we have generalized from Rappaport who included only the effects of gravity g_α, to include the effects of meridional-plane winds and zonal electric fields

$$A_\alpha = g_\alpha + \nu_{in}U_\alpha - \nu_{in}E_\beta/B \tag{A8}$$

(ν_{in} is the ion-neutral collision frequency). The integrals extend from one end of a field line at 90 km altitude to the point at the other end at the same altitude; in the *E* region, the conductivity includes the contribution from the molecular ions. For the maximum growth rate, we assume that the radial mode number K_L is zero; note that the longitudinal mode number m then cancels out of the formula. The damping effect of recombination can be included, following *Sultan* [1996], by subtracting from γ a flux-tube averaged rate $R = I(Ln)/I(n)$, where L is the local recombination rate.

[32] To apply the growth-rate formula in a more realistic geomagnetic field geometry, we perform the flux-tube integrations along the field lines traced from the IGRF field model. The scale factors h_α, h_β, and h_δ are estimated numerically by calculating the distances between points on adjacent field lines, where α and β identify the altitude and longitude, respectively, of the apex of the field line, and the scalar potential of the IGRF magnetic field serves as δ, to identify the position of the point along the field line.

[33] **Acknowledgments.** We thank R. Woodman for kindly providing us the Jicamarca data. We thank Odile de la Beaujardiere, J. Whalen, B. Basu, W. Burke, and J. Jasperse for interesting discussions and helpful comments on the manuscript. This research is partially supported by the Air Force Office of Scientific Research. The work at Utah State was supported by the Aeronomy Program, Division of Atmospheric Sciences of the National Science Foundation through grant ATM0004380. The Jicamarca Radio Observatory is operated by the Geophysical Institute of Peru, Ministry of Education, with support from the National Science Foundation as contracted through Cornell University.

[34] Arthur Richmond thanks David Anderson and Joseph Huba for their assistance in evaluating this paper.

References

Anderson, D. N. (1973), A theoretical study of the ionospheric F-region equatorial anomaly, I. Theory, *Planet. Space Sci.*, *21*, 409.

Basu, B., and B. Coppi (1983), Localized plasma depletion in the ionosphere and the equatorial spread *F*, *Geophys. Res. Lett.*, *10*, 900.

Brace, L. H., and R. F. Theis (1981), Global empirical models of ionospheric electron temperatures in the upper F-region and plasmasphere based on in situ measurements from the Atmospheric Explorer-C, ISIS 1, and ISIS 2 satellites, *J. Atmos. Terr. Phys.*, *43*, 1317.

de la Beaujardiere, O., et al. (2004), C/NOFS: A mission to forecast scintillations, *J. Atmos. Sol. Terr. Phys.*, *66*, 1573, doi:10.1016/j.jastp.2004.07.030.

Farley, D. T. (1991), Early incoherent scatter observations at Jicamarca, *J. Atmos. Terr. Phys.*, *53*, 665.

Farley, D. T., B. B. Balsey, R. F. Woodman, and J. P. McClure (1970), Equatorial spread *F*: Implications of VHF radar observations, *J. Geophys. Res.*, *75*, 7199.

Fejer, B. G. (1991), Low latitude electrodynamic plasma drifts: A review, *J. Atmos. Terr.*, *53*, 677.

Fejer, B. G., and L. Scherliess (1997), Empirical models of storm time equatorial zonal electric fields, *J. Geophys. Res.*, *102*, 24,047.

Fejer, B. G., E. R. de Paula, S. A. Gonzalez, and R. F. Woodman (1991), Average vertical and zonal F region plasma drifts over Jicamarca, *J. Geophys. Res.*, *96*, 13,901.

Fejer, B. G., L. Scherliess, and E. R. dePaula (1999), Effects of the vertical plasma drift velocity on the generation and evolution of equatorial spread *F*, *J. Geophys. Res.*, *104*, 19,859.

Haerendel, G., J. V. Eccles, and S. Cakir (1992), Theory for modeling the equatorial evening ionosphere and the origin of the shear in the horizontal plasma flow, *J. Geophys. Res.*, *97*, 1209.

Hedin, A. E. (1987), MSIS-86 thermospheric model, *J. Geophys. Res.*, *92*, 4649.

Hedin, A. E., et al. (1991), Revised global model of thermosphere winds using satellite and ground-based observations, *J. Geophys. Res.*, *96*, 7657.

Hinteregger, H. (1981), Observational, reference, and model data on solar EUV, from measurements on AE-E, *Geophys. Res. Lett.*, *8*, 1147.

Jasperse, J. (1974), Electron distribution function and ion concentrations in the earth's lower ionosphere from Boltzmann-Fokker-Planck theory, *Planet. Space Sci.*, *25*, 743.

Kelley, M. C. (1989), *The Earth's Ionosphere: Plasma Physics and Electrodynamics*, Elsevier, New York.

McClure, J. P., D. T. Farley, and R. Cohen (1970), Ionospheric electron concentration measurements at the magnetic equator, *ESSA Tech. Rep. ERL 186-AL4*, NOAA, Boulder, Colo.

Morse, P. M., and H. Feshbach (1953), *Methods of Theoretical Physics*, p. 21, McGraw-Hill, New York.

Ossakow, S. L. (1981), Spread-F theories: A review, *J. Atmos. Terr. Phys.*, *43*, 437.

Preble, A. J., D. N. Anderson, B. G. Fejer, and P. H. Doherty (1994), Comparison between calculated and observed *F* region electron density profiles at Jicamarca, Peru, *Radio Sci.*, *29*, 857.

Rappaport, H. L. (1996), Field line integration and localized modes in the equatorial spread *F*, *J. Geophys. Res.*, *101*, 24,545.

Retterer, J. M. (1999), Theoretical model for fast equatorial bubbles, in *Proceeding of the 1999 Ionospheric Effects Symposium*, edited by J. M. Goodman, p. 688, Off. of Naval Res., Arlington, Va.

Sales, G. (1999), Preliminary report on equatorial digisonde observations and the prediction of satellite scintillation events, paper presented at C/NOFS PI Meeting, Air Force Res. Lab., Hanscom Air Force Base, Mass.

Scherliess, L., and B. G. Fejer (1999), Radar and satellite global equatorial *F* region vertical drift model, *J. Geophys. Res.*, *104*, 6829.

Sultan, P. J. (1996), Linear theory and modeling of the Rayleigh-Taylor instability leading to the occurrence of equatorial spread *F*, *J. Geophys. Res.*, *101*, 26,875.

Woodman, R. F., and T. Hagfors (1969), Methods for the measurement of vertical ionospheric motions near the magnetic equator by incoherent scattering, *J. Geophys. Res.*, *74*, 1205.

Woodman, R. F., and C. LaHoz (1976), Radar observations of *F* region equatorial irregularities, *J. Geophys. Res.*, *81*, 5447.

Zalesak, S. T., S. L. Ossakow, and P. K. Chaturvedi (1982), Nonlinear equatorial spread *F*: The effect of neutral winds and background Pedersen conductivity, *J. Geophys. Res.*, *87*, 151.

W. S. Borer, D. T. Decker, and J. M. Retterer, Space Vehicles Directorate, Air Force Research Laboratory, Hanscom Air Force Base, MA 01731, USA. (john.retterer@hanscom.af.mil)

R. E. Daniell Jr., Computational Physics, Inc., 8001 Braddock Road, Suite 210, Springfield, VA 22151, USA.

B. G. Fejer, Center for Space Sciences, Utah State University, Logan, UT 84322, USA.